Science Advances

AAAS

advances.sciencemag.org/cgi/content/full/3/3/e1601552/DC1

Supplementary Materials for

From time-resolved atomic-scale imaging of individual donors to their cooperative dynamics

Philipp Kloth and Martin Wenderoth

Published 10 March 2017, *Sci. Adv.* **3**, e1601552 (2017)
DOI: 10.1126/sciadv.1601552

The PDF file includes:

Other Supplementary Material for this manuscript includes the following:
(available at advances.sciencemag.org/cgi/content/full/3/3/e1601552/DC1)

- movie S1 (.mp4 format). Spatiotemporally resolved decay of $dI(t_d)$ at the dopants in Fig. 2A.

section S1. Evolution of the space charge region when varying the z-height of the STM tip

In Fig. 1B in the main text, the change of $dI(t_d)$ spectra is discussed for increasing tunnel currents. For a current change from 150 to 2500 pA, the STM tip approaches 1-2 Å towards the sample surface (assuming a usual tunnel barrier height of 4 eV). With this variation in the tip height, also a variation in the tip-induced potential can be expected. fig. S1A-C shows the evolution of the SCR when the tip height above the surface is changed from 8 to 6 Å (doping density n_D=3e^{18}/cm^3, sample voltage 1.0 V, tip radius 30 nm). For this analysis, we used a commercial Poisson solver (COMSOL). Qualitatively, the size of the SCR varies only little.

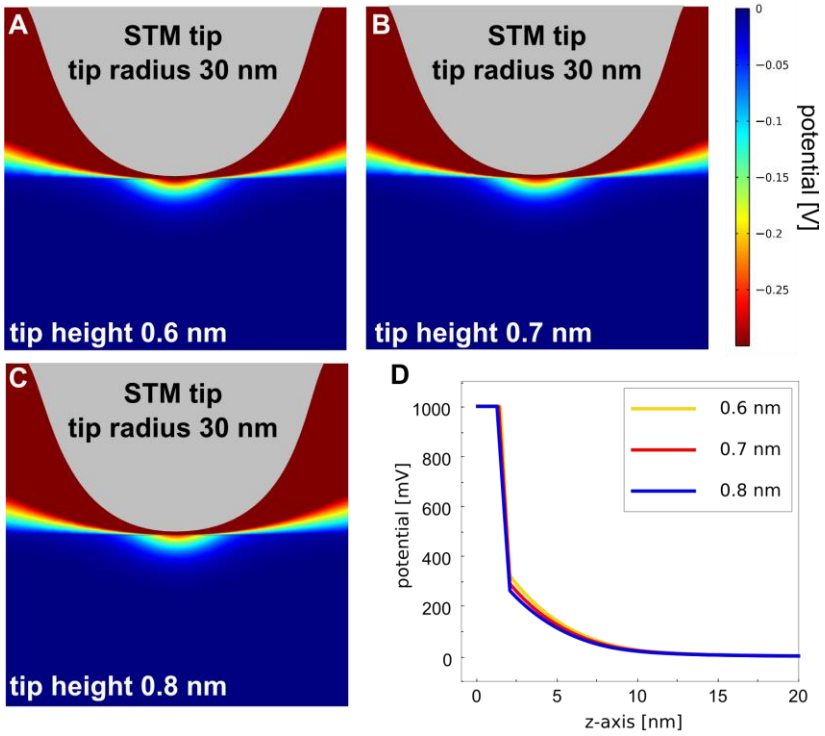

fig. S1. Calculation (Poisson solver) of the tip-induced potential for varying tip heights above the GaAs surface. (**A-C**) Spatial resolved potential (plotted color coded) for tip height of 0.6, 0.7 and 0.8 nm (doping density n_D=3e^{18}/cm^3, sample voltage 1.0 V, tip radius 30 nm). (**D**) Cross-sectional plot of the potential along the z-axis and in the middle of the STM tip.

For a more quantitative comparison, the fig. S1D demonstrates the change of the SCR in a cross-sectional plot of the induced potential along the *z*-axis starting at the center of the STM tip. The spatial extension of the SCR is for all heights roughly 10 nm. The absolute tip-induced potential at the surface varies, when going from 6 to 8 Å, only by 60 mV. Concluding, it can be stated, that the z-movement of the STM tip for the data in Fig. 1B is negligible.

section S2. Detecting the donor ionization process

In case of high currents I_0, photo-generated holes at the surface decay fast, leading to a small decay constant τ_{hole}. If the relaxation time of the donors is longer, the imbalance between τ_{hole} and τ_{don} will lead to interesting charge configurations. In the following we discuss the time evolution of the hole and ionized donor concentration upon and after pulsed excitation combined with the corresponding tunnel currents I_V and I_C (fig. S2A) and screening conditions sketched in tunneling band schemes (fig. S2B-E).

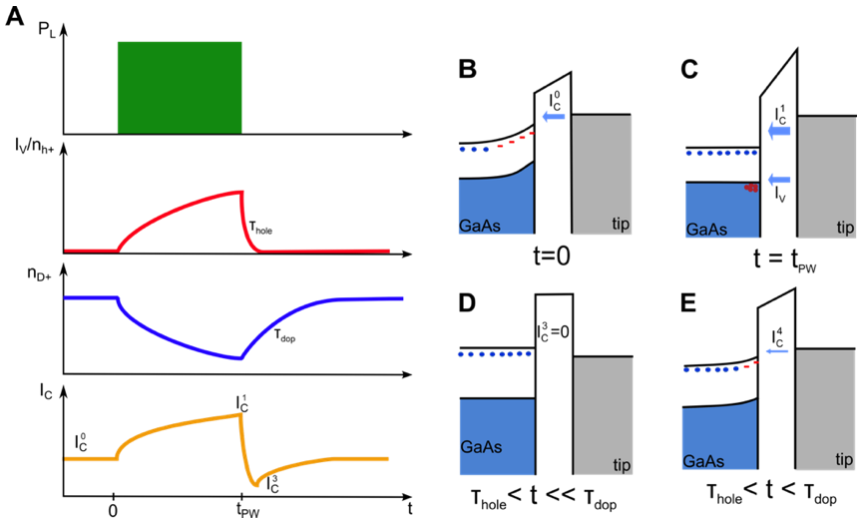

fig. S2. Real-time evolutions of experimental parameters (hole density, ionized dopant density, and conduction band tunneling) at high tunnel currents and the corresponding screening configurations sketched in band schemes. (**A**) Laser intensity P_L, hole concentration (valence band tunneling) n_{h+}, I_V, concentration of ionized donors at the surface n_{D+} and conduction band tunneling I_C plotted in real time in case of fast hole annihilation. (**B-E**) Screening configurations at characteristic time points sketched in tunneling band schemes.

Under dark conditions (fig. S2B, t=0) tip-induced band bending with the charge provided by ionized dopants is found. The conduction band tunneling I_C^0 is given by the set point. Upon excitation ($0<t<t_{PW}$) holes accumulate at the surface increasing the hole concentration n_{h+} and leading to valence band tunneling I_V (fig. S2C). Simultaneously, the concentration of ionized dopants n_{D+} decreases by electron capturing and the more efficient screening of the tip potential leads to an increase of I_C^1 (fig. S2C). At $t> t_{PW}$ for high currents, I_V and also n_{h+} decay fast. Under extreme conditions, all holes at the surface have disappeared but yet no dopant has ionized (fig. S2D). Consequently charge is missing at the surface and during these temporary non-equilibrium conditions the voltage drop over the vacuum barrier gets small and likewise the conduction band tunneling vanishes (I_C^3=0) resulting in a negative dI. Eventually the remaining neutral donors at the surface ionize and the system relaxes back to its ground state (fig. S2E). The exponential decay for negative dI gives us access to the time characteristics of these donor charging events.

section S3. Exemplary fitting results of $dI(t_d)$ curves of Fig. 1E

In order to extract the current-dependency of the $dI(t_d)$ spectra, shown in Fig. 1E, we conducted exponential fitting routines. Two exemplary results for low and high tunnel currents are shown in fig. S3.

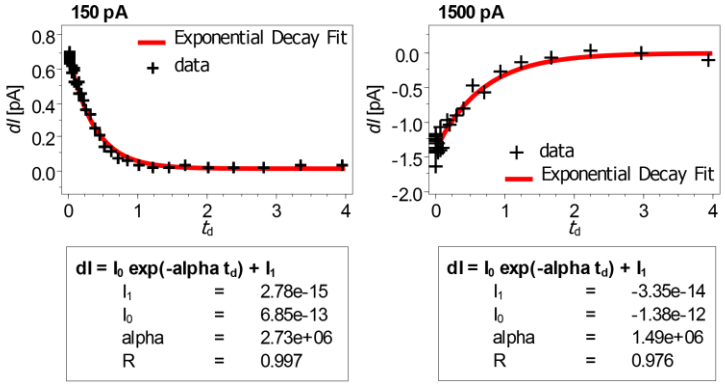

fig. S3. Two exemplary fitting results of the $dI(t_d)$ spectra of Fig. 1E. The parameter R stands for the nonlinear regression coefficient. The other parameters are self-descriptive.

Please note, that in these two spectra one isolated decaying process is visible. In the transition region (450-550 pA) we applied fittings of single exponential decaying function. In this case, we restricted the fitting region to correspondent early and late decay time points t_d of the processes (fig. S4).

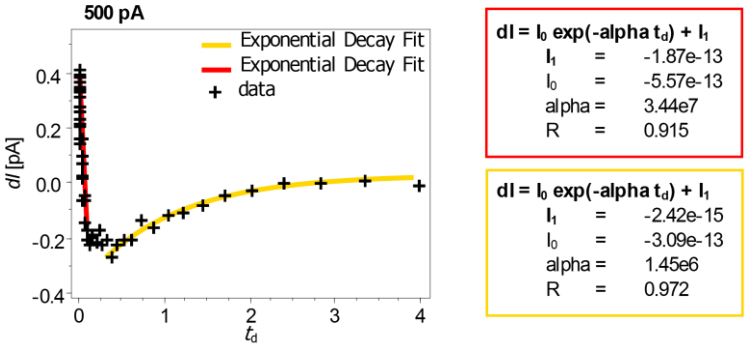

fig. S4. Exemplary fitting results of the $dI(t_d)$ spectra of Fig. 1E in the transition region. In this case the fitting is restricted to early (red) and late (yellow) delay times. The parameter R stands for the nonlinear regression coefficient. The other parameters are self-descriptive.

section S4. Logarithmic analysis of the decay spectra of Fig. 2B

In order to ensure the exponential dependency in the spectra in Fig. 2B, the data is additionally plotted on a logarithmic scale (fig. S5).

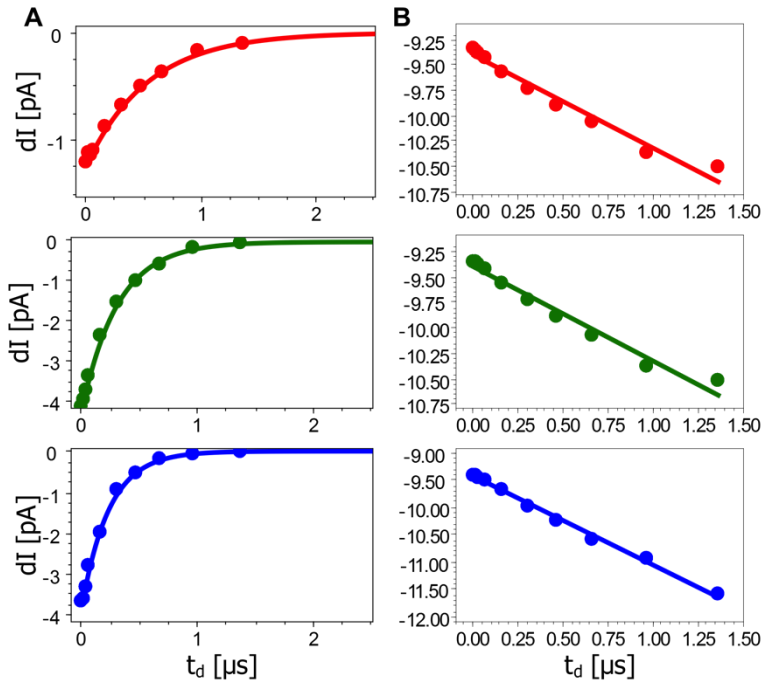

fig. S5. Decay spectra of Fig. 2B of the main manuscript plotted on normal and logarithmic scale. The color assignment is identical to the main manuscript.

For the sake of clarity, the data is plotted another time on normal scale (fig. S5A). Please note that the color assignment is identical to the assignment in the main manuscript. Figure S5B shows the same spectra, plotted on a logarithmic scale. In a first approximation, the assumption of an exponential dependency is sensible.

section S5. Determining the donor depth

In order to attribute τ_{don} to a binding energy in Fig. 2D, it is necessary to determine the exact depth of the donor. In a first step we order the donors correspondingly to their signature height in the topography (fig. S6A). The surface nearest dopant induces the highest change in the tip height (red dot) whereas the deeper ones show a modulation in tip height, which monotonically decreases (green and then the blue dot) with the depth. For a more exact determination of the donor position we use the stacking sequence of the GaAs atomic layers at the (110) surface. We extract the point of maximum modulation in the topography for each dopant signature and assume that this point is positioned centered above the buried doping atom.

Having an ABAB stacking sequence at the GaAs(110) surface this point is either positioned on a corrugation maximum (even) or next to it (odd), i.e. in between two maxima (fig. S6B). With this information we can assign to each donor signature in the topography its position in an even or odd layer beneath the surface (fig. S6C). With this information and with the help of comparable, previous studies, performed in our workgroup, we are able to determine the exact depth of the dopant.

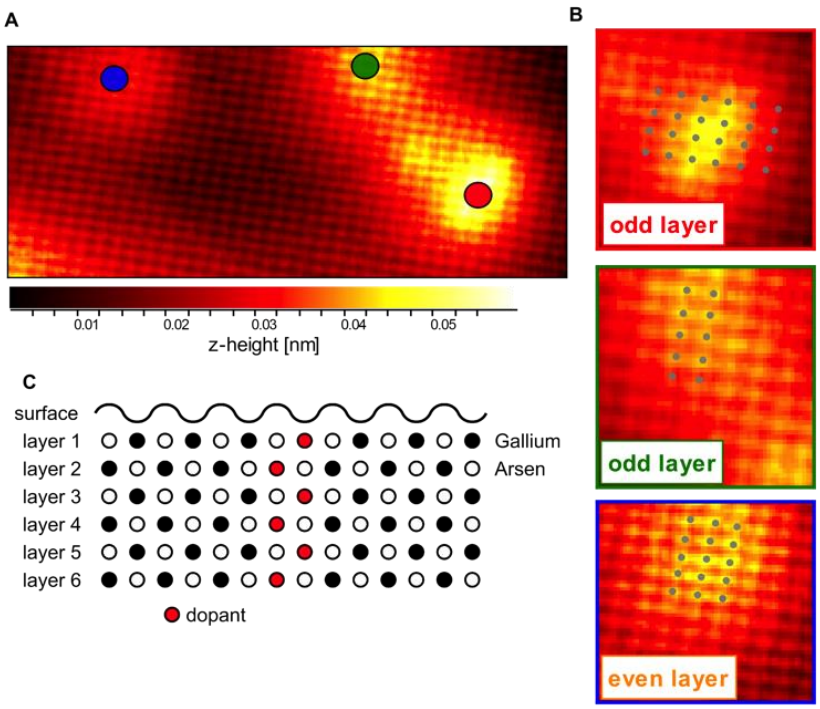

fig. S6. Extracting the dopant depth from STM topographies. (**A**) STM topography showing the signature of three buried dopants. Depending on the depth, the z-height modulation above the dopant decreases. (**B**) More detailed pictures of each single dopant labeled in red, green and blue in A. Grey points trace the atomic corrugation. (**C**) ABAB stacking at the GaAs(110) surface. Red dot: layer 1, Green dot: layer 3, Blue dot: layer 4.

section S6. Temperature-dependent analysis of the dopant charging

Two possible mechanisms for the dopant ionization have been considered to describe the spatial variation of decay time for the electron release from the donor level: thermal emission and field-driven tunneling of electrons into the conduction band. In order to probe for thermal emission we conducted time spectra at 6 K (blue line) and 77 K (red line). Plotted (fig. S7) is the normalized SPPX induced current *dI* against the delay time t_d.

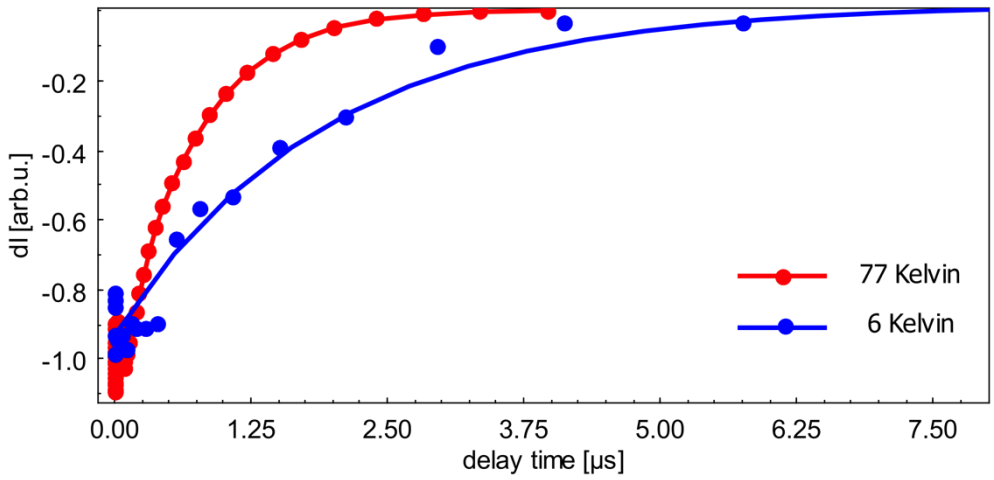

fig. S7. Dopant relaxations, given in *dI*, plotted against the delay time t_d, for different temperatures. Red line: Decay at 77 K gives τ_{don}=711 ns (1 V bias voltage, 1500 pA set point current, exc. parameters: 40 ns pulse width, 8 µs rep. cycle, 8 µW average power). Blue line: Decay at 6 K gives τ_{don}=2 µs (2 V bias voltage, 400 pA set point current, exc. parameters: 400 ns pulse width, 32 µs rep. cycle, 20 µW average power).

At 77 K (red line) the dopant decay time τ_{don}(77 K) is given by 711 ns whereas at 6 K it takes τ_{don}(6 K)=2 µs to relax to the ground state. Theoretically the ratio $R=\tau_{don}^{T_1}/\tau_{don}^{T_2}$ at temperatures T_1 and T_2 in case of thermal emission can be estimated by

$$\mathrm{R} = \frac{\tau_{don}^{T_1}}{\tau_{don}^{T_2}} = \frac{\exp(-\frac{E_B}{k_B T_1})}{\exp(-\frac{E_B}{k_B T_2})}$$

With a binding energy of 45 meV, the ratio R for T_1=77 K and T_2= 6 K would be large ($R \sim 10^{35}$). This contradicts our experimental finding and we conclude that thermal emission is not a relevant process in our case. The difference in the relaxation time τ_{dop} in fig. S7 may originate from the different set point or excitation parameters. A further understanding demands for spatially resolved 6 K measurements.

section S7. Field-driven tunnel ionization from the donor level into the conduction band

We propose field-driven tunnel ionization as the relaxation mechanism of excited, neutral dopants. Figure S8 sketches the situation schematically. The tip-induced potential $\Delta\phi$ at the GaAs surface pulls the conduction band edge below the donor level enabling this process. Two parameters are crucial for the tunneling probability: the electric field $\boldsymbol{E}$ at the donor position and the binding energy E_B of the electron in the donor level.

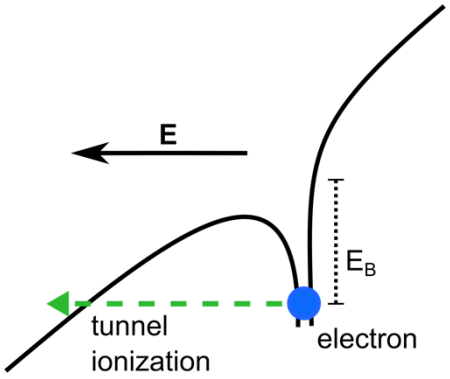

fig. S8. Schematic for field-driven tunnel ionization. The tunneling rate from the donor level into the conduction band is defined by the tip-induced electric field $\boldsymbol{E}$ at the dopant position and the binding energy E_B.

As a quantitative model for the charging rate $\omega = \frac{1}{\tau_\mathrm{hydro}}$ we use the analytical expression for the ionization process of a hydrogen atom in an electric field $\boldsymbol{E}$(25)

$$\omega = 4\omega_\mathrm{A}\,\frac{E_\mathrm{A}}{|\boldsymbol{E}|}\,\mathrm{e}^{-\frac{2}{3}\frac{E_\mathrm{A}}{|\boldsymbol{E}|}}$$

Adapting this expression to the hydrogen-like donor level of silicon in bulk GaAs the parameters ω_A and E_A become

$$\omega_\mathrm{A} = \frac{m_\mathrm{e}\, m^*\, e^4}{(4\pi\varepsilon_0\varepsilon_\mathrm{r})^2\hbar^3}\,,\; E_\mathrm{A} = \frac{2\, m_\mathrm{e}\, m^*\, e^2\, E_\mathrm{B}}{4\pi\,\varepsilon_0\varepsilon_\mathrm{r}\,\hbar^2}$$

with $m^* = 0.06$ and ε_r =12.8. The other notations are standard values.

section S8. Making a movie of $dI(t_d)$, spatially resolved

A part of the supplemental materials includes a movie, showing the spatiotemporal-resolved decay of the optical induced signal $dI(t_d)$ at the three donors in Fig. 2A. In order to reduce the measuring time of time-resolved maps, limited by experimental parameters like drift of the STM tip or cryostat hold time of cold gases, we used only ten delay points in the data set. However, in order to animate $dI(t_d)$ spatially, we performed exponential fittings at each single spectra taken in Fig. 2A via the formula:

$$dI(t_d) = dI_0 \exp\left(-\frac{1}{\tau}\, t_d\right)$$

With the fitting results we are able to interpolate the time steps between our discrete delay times. The result can be seen in the attached movie *SM1*.